

O/F anion order in $\text{Pb}_2\text{Ti}_4\text{O}_9\text{F}_2$ stabilized by the $6s^2$ lone pair electrons of Pb^{2+}

Kengo Oka*

*Department of Applied Chemistry, Faculty of Science and Engineering,
Kindai University, Higashiosaka, Osaka 577-8502, Japan*

Tom Ichibha†

Materials Science and Technology Division, Oak Ridge National Laboratory, Oak Ridge, Tennessee 37831, USA

Daichi Kato

Department of Energy and Hydrocarbon Chemistry, Graduate School of Engineering, Kyoto University, Kyoto 615-8510, Japan

Mitsunobu Iwasaki

*Department of Applied Chemistry, Faculty of Science and Engineering,
Kindai University, Higashiosaka, Osaka 577-8502, Japan*

Naoki Noma

Joint Research Center, Kindai University, Higashiosaka, Osaka 577-8502, Japan

Kenta Hongo

*Research Center for Advanced Computing Infrastructure,
JAIST, Asahidai 1-1, Nomi, Ishikawa 923-1292, Japan*

Ryo Maezono

School of Information Science, JAIST, Asahidai 1-1, Nomi, Ishikawa 923-1292, Japan

Fernando A. Reboredo

Materials Science and Technology Division, Oak Ridge National Laboratory, Oak Ridge, Tennessee 37831, USA

Understanding the mechanisms of anionic ordering in mixed anion compounds is a crucial factor for designing their structural and functional properties. Some oxyfluorides are known to exhibit the F^- ordering. The ordering is accompanied by a tetragonal distortion, which is believed to be originated by the $6s^2$ lone pairs of Bi and Pb. To elucidate the role played by the lone pair, we studied isostructural $\text{Bi}_2\text{Ti}_4\text{O}_{11}$ and $\text{Pb}_2\text{Ti}_4\text{O}_9\text{F}_2$ with a combination of synchrotron X-ray diffraction techniques and ab initio calculations. $\text{Bi}_2\text{Ti}_4\text{O}_{11}$ undergoes antiferroelectric-paraelectric transitions from $C2/c$ to $C2/m$. Meanwhile, $\text{Pb}_2\text{Ti}_4\text{O}_9\text{F}_2$ does not, because F^- selectively occupies the closest anion site to Bi/Pb and reduces the distortion. The question on why a particular site is selectively occupied by F^- in $\text{Pb}_2\text{Ti}_4\text{O}_9\text{F}_2$ becomes important to understand the role of $6s^2$ lone pair electrons for stabilizing the anion order. Our DFT ab initio calculations reproduced the same anionic arrangement in terms of the total energy. However, this energy gain cannot be fully explained by the electrostatic (Madelung) potential alone, being an exception of the Pauling's second rule. We explain the reason focusing on the steric effects of $6s$ lone pairs.

This manuscript has been authored by UT-Battelle, LLC, under Contract No. DE-AC05-00OR22725 with the US Department of Energy (DOE). The US Government retains and the publisher, by accepting the article for publication, acknowledges that the United States Government retains a nonexclusive, paid-up, irrevocable, worldwide license to publish or reproduce the published form of this manuscript, or allow others to do so, for US Government purposes. Ichibha provided a large part of the calculation results. Ichibha and Fernando wrote the paper coworking with the other authors. DOE will provide public access to these results of federally sponsored research in accordance with the DOE Public Access Plan (<http://energy.gov/downloads/doe-public-access-plan>).

I. INTRODUCTION

The properties of mixed anion compounds strongly depend on the degree of order or disorder of the anions. Anionic ordering can cause heteroleptic coordinations or low-dimensional structure which in turn modify electronic prop-

erties. This intriguing possibility to modify a material has attracted significant attention [1–4]. A typical example are ABX_3 perovskites. For example, SrTaO_2N and BaTaO_2N have a high dielectric constant due to the O/N anion order [5–7]. In addition, an oxyhydride SrVO_2H shows the two-dimensional electronic conduction and compression anisotropy due to the O/H anion order [8].

Multiple anions and cations are heteroleptically coordinated and their concentrations typically obey valence charge neutrality conditions. When differences in ionic

* koka@apch.kindai.ac.jp; These two authors contributed equally.

† ichibha@icloud.com; These two authors contributed equally.

radii, electronegativity or polarizability are large, materials tend to exhibit ionic ordering. However, although O^{2-} and F^- are neighboring anions in the periodic table, the oxyfluorides exhibit an anionic ordering depending on the structure. While simple cubic perovskites ($SrFeO_2F$ [9], $BaFeO_2F$ [10], $PbScO_2F$ [11], $BaScO_2F$ [12], $AgFeOF_2$ [13], $BaInO_2F$ [14], and $AgTiO_2F$ [15]) adopt disordered configurations, a variety of Ruddlesden-Popper type layered perovskites ($Sr_2CuO_2F_2$ [16], Sr_2FeO_3F [17, 18], Ba_2InO_3F [19], Ba_2ScO_3F [20], Sr_2MnO_3F [21], $Sr_3Fe_2O_{5-x}F_y$ [17, 22]) exhibit ordered configurations of F^- [23]. In layered perovskites, multiple distinct anion sites are present and support anion order. This manner can be interpreted by considering the Pauling's second rule, where a stable ionic structure is arranged to compensate the valence of an anion by the bond strength of coordinated cations. Thus, F^- prefers more open site compared to O^{2-} , leading to O/F anion order. However, in spite of a simple perovskite, partial anion order is reported for $PbFeO_2F$, accompanied with a tetragonal distortion [24, 25]. The anisotropic instability observed in this and similar systems ($PbTiO_3$ [26], $Pb(Zr_xTi_{1-x})O_3$ [27], and $BiFeO_3$ [28]), has been attributed to the existence of a the $6s^2$ lone pair.

To investigate the role played by the $6s^2$ lone pair, we concentrate on the oxyfluorides containing Pb or Bi [29–31]. For an ideal analysis, completely isostructural oxyfluoride and oxide (as a reference) would be desirable, though such a pair of compounds are rarely found. Pyrochlore oxyfluoride and oxide, $Pb_2Ti_2O_{5.4}F_{1.2}$ and $Bi_2Ti_2O_7$ [32], would have the right stoichiometry, but these compounds belong to different space groups [$Pb_2Ti_2O_{5.4}F_{1.2}$ ($Fd-43m$) and $Bi_2Ti_2O_7$ ($Fd-3m$)]. Another candidate would be $PbOF_2$ and Bi_2O_3 , since $PbOF_2$ adopts a similar structure to β - Bi_2O_3 [33], but they also belong to different space groups [$PbOF_2$ ($P4_2/nmc$) and β - Bi_2O_3 ($P-42_1c$)].

Eventually, we found an isostructural pair $Pb_2Ti_4O_9F_2$ [30] and oxide $Bi_2Ti_4O_{11}$ [34]. Both Pb^{2+} and Bi^{3+} have the same electron configuration and a $6s^2$ lone pair. $Bi_2Ti_4O_{11}$ undergoes antiferroelectric-paraelectric transitions from $C2/c$ to $C2/m$, while $Pb_2Ti_4O_9F_2$ does not. The high-temperature paraelectric phase of $Bi_2Ti_4O_{11}$ ($C2/m$) adopts the same space group symmetry as $Pb_2Ti_4O_9F_2$ [34]. Thus, the system provides ideal platform to investigate the role of $6s^2$ lone pair on O/F anion arrangement.

An earlier work by Oka et al. found that F^- selectively occupies the closest anionic site to Bi/Pb site in $Pb_2Ti_4O_9F_2$. [30]. The anionic site was named site-6. They observed that the fluorine occupation elongates the distance between the site-6 and Bi/Pb site. Oka et al. concluded that the elongation caused the disappearance of antiferroelectric transition in $Pb_2Ti_4O_9F_2$.

In this paper, to understand what is unique at site-6, we carefully analyzed the comparison with the reference, $Bi_2Ti_4O_{11}$ [34], to find that the site has a structural instability toward anisotropy due to the $6s^2$ lone pair. In $Bi_2Ti_4O_{11}$, the instability leads to the anisotropic coordination to provoke the transition toward antiferroelectricity. The instability

generated by the lone pair causes site-6 to be the preferred site for F^- in $Pb_2Ti_4O_9F_2$. To understand this preference, we performed ab initio calculations. Though the total energy is surely stabilized by the site-6 occupation, it is not fully stabilized due to the electrostatic (Madelung) potential, being an exception of the Pauling's second rule. Our structural and bonding nature analyses showed that the site-6 occupation weakens the anti-bonding orbital, between Pb and site-6 anion, distributing on the other side of the site-6 across Pb. The change of the anti-bonding orbital reduces the steric effect that hampers Pb to bond with the site-2 oxygen on the other side of the site-6. This can be the reason of the deviation from the Pauling's second rule.

We organize the rest of the paper as follows. In Section II, we describe the details of the synthesis and synchrotron X-ray powder diffraction (SXRD) and the calculation conditions. In Section III, we compare and discuss the geometric and electronic structures of $Pb_2Ti_4O_9F_2$ with the isostructural oxide, the high-temperature (HT) phase of $Bi_2Ti_4O_{11}$, and the low-temperature (LT) phase of $Bi_2Ti_4O_{11}$. In Section IV, we show the total energies and electrostatic energies for the possible five anion orders to show that their lowest energies structures are inconsistent. This is not explained by the Pauling's second rule. We discuss the reason focusing on the orbital hybridizations. We summarize our work in Section V.

II. METHODS

The powder samples of $Bi_2Ti_4O_{11}$ and $Pb_2Ti_4O_9F_2$ were prepared by solid-state reaction as previously reported [30, 34]. $Bi_2Ti_4O_{11}$ was synthesized from a stoichiometric mixture of Bi_2O_3 (99.9%, Rare Metallic Co.) and TiO_2 (99.9%, Rare Metallic Co.) powders. The pelletized mixture was treated at 1273 K for 12 h in the air. $Pb_2Ti_4O_9F_2$ was synthesized from a mixture of PbO (99.9%, Rare Metallic Co.), PbF_2 (99.9%, Rare Metallic Co.) and TiO_2 (rutile, 99.9%, Rare Metallic Co.) powders were weighed to be slightly fluorine-rich to compensate the loss of fluorine during the reaction. The pelletized mixture was sealed in an evacuated Pyrex tube and treated at 823 K for 12 h.

SXRD patterns were collected with a large Debye–Scherrer camera installed at beamline BL02B2 of SPring-8 using a glass capillary and a solid state detector [35]. The crystallographic parameters were refined by the Rietveld method using the RIETAN-FP program [36]. The electron density distributions were determined by the maximum entropy method (MEM) using the Dynomia program [37]. The crystal structures and electron density mappings are visualized using VESTA program [38].

The density functional theory (DFT) calculations were performed with Quantum Espresso [39]. Perdew–Burke–Ernzenhof semi-local functional [40] was employed. The core orbitals were described by projector augmented wave method [41]. The valence orbitals were expanded with plane waves. The cutoff energy was 100 Ry and the k -point mesh was $7 \times 7 \times 5$ for the unit cell. The LOBSTER code [42] was

used to calculate Mulliken and Löwdin charges and perform the Madelung potential and the Crystal Orbital Hamiltonian Population (COHP) analyses based on the DFT results with pbeVaspFit2015 basis set [43, 44].

III. COMPARISON BETWEEN $\text{Bi}_2\text{Ti}_4\text{O}_{11}$ AND $\text{Pb}_2\text{Ti}_4\text{O}_9\text{F}_2$

Production of single phase for both $\text{Bi}_2\text{Ti}_4\text{O}_{11}$ and $\text{Pb}_2\text{Ti}_4\text{O}_9\text{F}_2$ samples were confirmed by SXRD technique. $\text{Bi}_2\text{Ti}_4\text{O}_{11}$ undergoes structural transition from low-temperature (LT) antiferroelectric (Space group: $C2/c$) to high-temperature (HT) paraelectric phase (Space group: $C2/m$) at 506 K [34]. As previously reported, $\text{Pb}_2\text{Ti}_4\text{O}_9\text{F}_2$ is isostructural with the HT paraelectric phase of $\text{Bi}_2\text{Ti}_4\text{O}_{11}$ and does not show structural transition down to 5 K [30]. Fig. 1 shows the SXRD patterns and results of Rietveld refinement for the LT (300 K) and HT (600 K) phases of $\text{Bi}_2\text{Ti}_4\text{O}_{11}$ and $\text{Pb}_2\text{Ti}_4\text{O}_9\text{F}_2$ (300 K) and illustrations of those crystal structures. The refinements reached convergence for all patterns. The refined crystallographic parameters are summarized in the supporting information.

The local coordination environments around Bi/Pb in $\text{Bi}_2\text{Ti}_4\text{O}_{11}$ and $\text{Pb}_2\text{Ti}_4\text{O}_9\text{F}_2$ are shown in Fig. 2. The numbers at the anions indicate the site indices. We provide the experimental crystal structures in the CIF format as the supporting information, as one can distinguish the anion sites with their own visualizing softwares. The shortest Bi/Pb-O/F6 bond lengths are largely different between $\text{Bi}_2\text{Ti}_4\text{O}_{11}$ and $\text{Pb}_2\text{Ti}_4\text{O}_9\text{F}_2$. Pb-F6 of $\text{Pb}_2\text{Ti}_4\text{O}_9\text{F}_2$ is significantly longer than Bi-O6 of the HT phase of $\text{Bi}_2\text{Ti}_4\text{O}_{11}$. Here, O6 (F6) indicates an oxygen (fluorine) ion in the site-6. The elongated bond length reduces the degree of anisotropy of the ligand configurations around Bi/Pb as shown in Figure 2. The antiferroelectric transition in $\text{Bi}_2\text{Ti}_4\text{O}_{11}$ is known to be associated with displacements of the Bi ion from the centrosymmetric position along the b axis [34, 45]. Therefore, the disappearance of antiferroelectric transition for $\text{Pb}_2\text{Ti}_4\text{O}_9\text{F}_2$ would be related to the reduced anisotropic character around Pb^{2+} ion.

The changes in local coordination environment around Bi^{3+} or Pb^{2+} were further investigated. Figure 3 shows the electron density distribution obtained by MEM. The differences of covalent character of the Bi-O6 bonds between the HT and LT phases of $\text{Bi}_2\text{Ti}_4\text{O}_{11}$ are obvious. This anisotropic change in covalency around Bi^{3+} is associated with the anti-parallel displacement of Bi^{3+} ion along the b axis in the LT phase, suggesting $6s^2$ lone pair electrons at play. Therefore, we infer that the absence of antiferroelectric transition in $\text{Pb}_2\text{Ti}_4\text{O}_9\text{F}_2$ is a consequence of the reduction on the interaction between the Pb-6s and anion-2p electrons. Fig. 4 shows a 2-dimensional electron density mapping sliced along Bi/Pb-O/F6 bond obtained by MEM. The electron density associated to the covalent character of Bi-O6 is observed in $\text{Bi}_2\text{Ti}_4\text{O}_{11}$ at the HT phase. On the other hand, the covalency between Pb and F6 is less pronounced in $\text{Pb}_2\text{Ti}_4\text{O}_9\text{F}_2$. These results suggest that O/F anion order in $\text{Pb}_2\text{Ti}_4\text{O}_9\text{F}_2$ occurs to reduce the interaction between 6s and 2p electrons.

We verified the experimental conclusion theoretically performing a COHP analysis to the hybrid orbital of Pb/Bi-6s and O/F-2p. The COHP analysis quantifies the degree of (anti-)bonding strength of the hybrid orbital evaluating the integrated COHP (ICOHP). Positive (negative) ICOHP indicates anti-bonding (bonding) nature. The absolute value indicates a degree of (anti-)bonding strength. We obtained $\text{ICOHP}(\text{Pb-6s} - \text{F6-2p}) = -0.032$ and $\text{ICOHP}(\text{Bi-6s} - \text{O6-2p}) = -0.289$: Pb-6s and F6-2p make a significantly weaker bonding hybrid orbital than Bi-6s and O6-2p, supporting the experimental conclusion.

TABLE I. Comparisons of the total energies for the different site occupations by F^- of $\text{Pb}_2\text{Ti}_4\text{O}_9\text{F}_2$. The F-in-site6 is taken as the reference for the energy deviations, ΔE , given in the unit of [eV/f.u.].

	ΔE
F-in-site1	2.038
F-in-site2	1.871
F-in-site4	0.642
F-in-site5	0.122
F-in-site6	0.000

IV. REASON OF THE F-IN-SITE6 PREFERENCE IN $\text{Pb}_2\text{Ti}_4\text{O}_9\text{F}_2$

We performed DFT ab initio calculations to evaluate the energetics of the F^- occupation patterns of $\text{Pb}_2\text{Ti}_4\text{O}_9\text{F}_2$. Table I shows the comparisons of the total energies, reproducing the experimental F-in-site6 preference. To understand the origin of F-in-site6 stabilization, we compared Madelung electrostatic potentials upon the Milliken and Löwdin charges, shown as the vertical axis values in Fig. 5. The total energies are roughly proportional to the electrostatic potentials, consistent with a previous systematic study on NdNiO_2F by simulations [46]. Meanwhile, the F-in-site6 cannot be fully explained by the Pauling's second law (structural stabilization via electrostatic gain), requiring us to investigate further the origin of the F-in-site6 stabilization.

TABLE II. Energy differences (F-in-site5 - F-in-site6) of the valence orbital channels.

Orbital channel	Energy (eV)
F-2s	+0.098
F-2p	-0.062
O-2s	-0.206
O-2p	+1.288
Pb-6s	+0.820
Pb-6p	+0.078
Ti-3s	+0.005
Ti-3p	+0.009
Ti-3d	+0.095
Ti-4s	+0.028
Total	+2.15

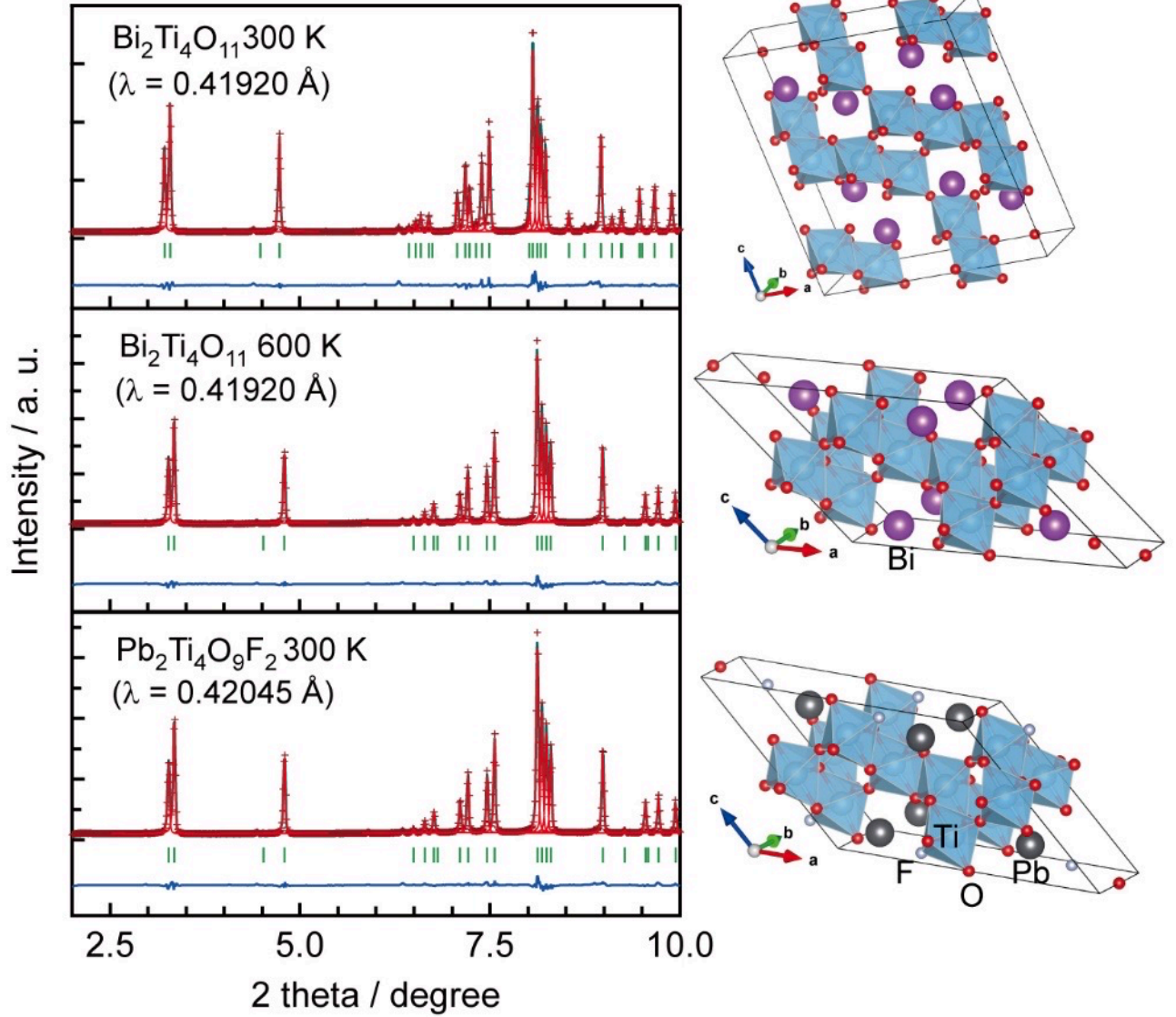


FIG. 1. Structural characterization of $\text{Pb}_2\text{Ti}_4\text{O}_9\text{F}_2$ and $\text{Bi}_2\text{Ti}_4\text{O}_{11}$ by Rietveld refinement using the SXRD patterns. The red crosses, black solid line, and blue solid line respectively represent the observed, calculated, and difference intensities. The green ticks indicate the positions of the Bragg peaks. The illustrations of refined crystal structures are shown at the right side.

We focused on the the orbital energies to explain the F-in-site6 stabilization. Figure 6 shows the PDOS for each F^- occupation pattern in $\text{Pb}_2\text{Ti}_4\text{O}_9\text{F}_2$. Except for F-in-site6, a peaky state of Pb-6s exists at the upper edge of the valence band, as indicated by the arrow. The peaky state signals the orbital hybridization described by the RLP model [47]. The result indicates that the hybridization occurred mainly between Pb and O6. The energy of orbital α is given as the integration of $\varepsilon \cdot D(\varepsilon)$, where $D_\alpha(\varepsilon)$ is the PDOS of the orbital α at the energy ε . We performed the PDOS integration for each orbital in the valence band range, [-10eV:0eV] ($\varepsilon=0$ eV is the Fermi energy). Then, we compared the orbital energy differences between F-in-site5 and F-in-site6, as shown in Table II: the

orbital energy of O-2p was significantly higher for F-in-site5 than F-in-site6.

TABLE III. Energy differences (F-in-site5 - F-in-site6) of the 2p channels of the anions.

α (orbital)	$\int \varepsilon \cdot \Delta D_\alpha(\varepsilon) d\varepsilon$
O1-2p	+0.119
O2-2p	+0.335
O3-2p	+0.015
O4-2p	-0.064
O5/6-2p+F6/5-2p	+0.191

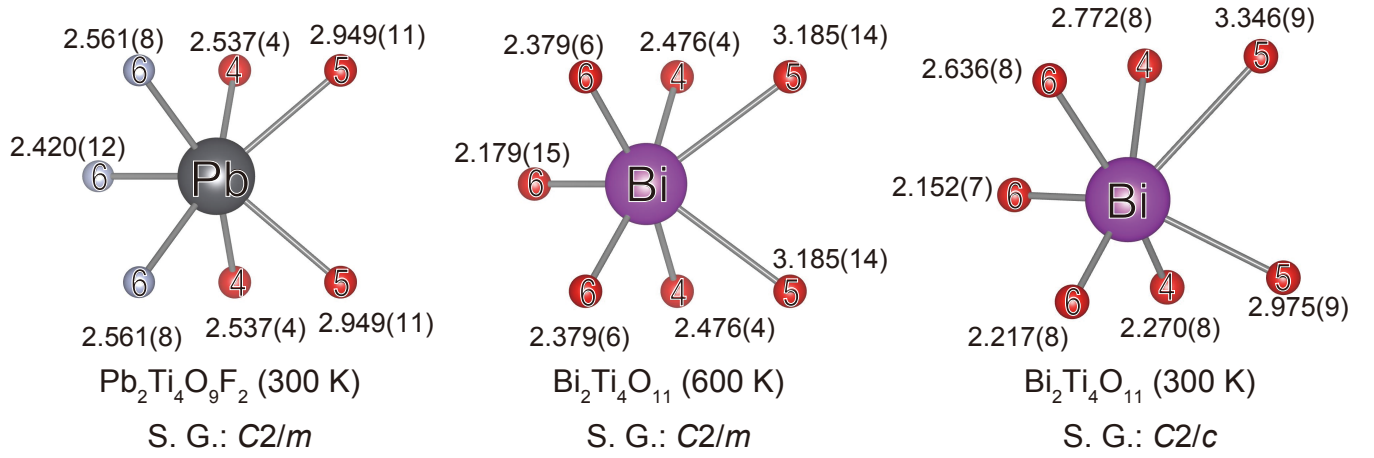


FIG. 2. Local coordination environments around Pb/Bi for $\text{Pb}_2\text{Ti}_4\text{O}_9\text{F}_2$ and $\text{Bi}_2\text{Ti}_4\text{O}_{11}$. The annotations mean the bond lengths (\AA) between Pb/Bi-O/F.

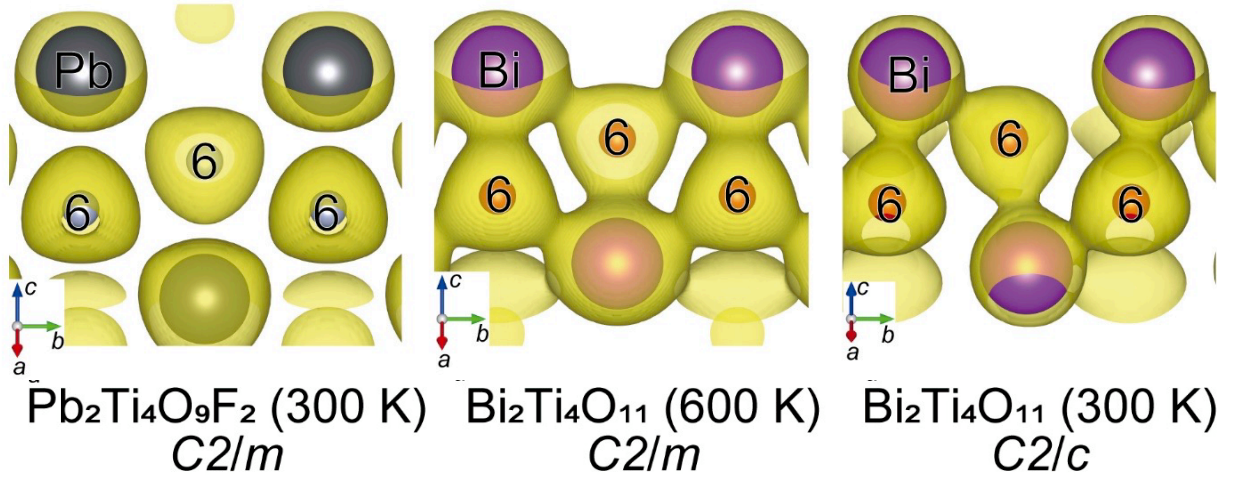


FIG. 3. Electron density distributions obtained by MEM for $\text{Pb}_2\text{Ti}_4\text{O}_9\text{F}_2$ and $\text{Bi}_2\text{Ti}_4\text{O}_{11}$. The isosurface level is $4 e/\text{\AA}^3$.

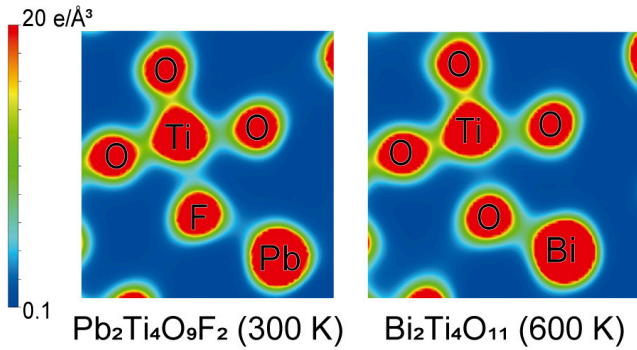


FIG. 4. 2D-electron density mapping sliced along (010) plane obtained by MEM for $\text{Pb}_2\text{Ti}_4\text{O}_9\text{F}_2$ and HT phase of $\text{Bi}_2\text{Ti}_4\text{O}_{11}$.

The $2p$ orbital energy difference of each oxygen between F-in-site5 and F-in-site6 is shown in Table III. (For sites 5 and 6, we compared $\text{O5-}2p + \text{F6-}2p$ for F-in-site5 and $\text{F5-}2p + \text{O6-}2p$ for F-in-site6.) The result shows that $2p$ orbital energy of O2 differs the most. O2 is located on the other side of O/F6 across the Bi/Pb as shown in Figure 7. The figure shows the distance and ICOHP between Pb and O2 and the values indicate weaker binding strength for the F-in-site5. This would be attributed to that the Pb-O6 hybridization for F-in-site5 is stronger than the Pb-F6 hybridization for F-in-site6. The hybridization makes an anti-bonding orbital distributing in the other side of the O/F6 across the Bi/Pb, i.e., between the Bi/Pb and O2. Therefore, the anti-bonding orbital caused by the $6s^2$ lone pair would hamper the binding between Bi/Pb and O2 as a steric effect. Since the hybridization is stronger for F-in-site5 than F-in-site6, the steric effect would be also stronger for F-

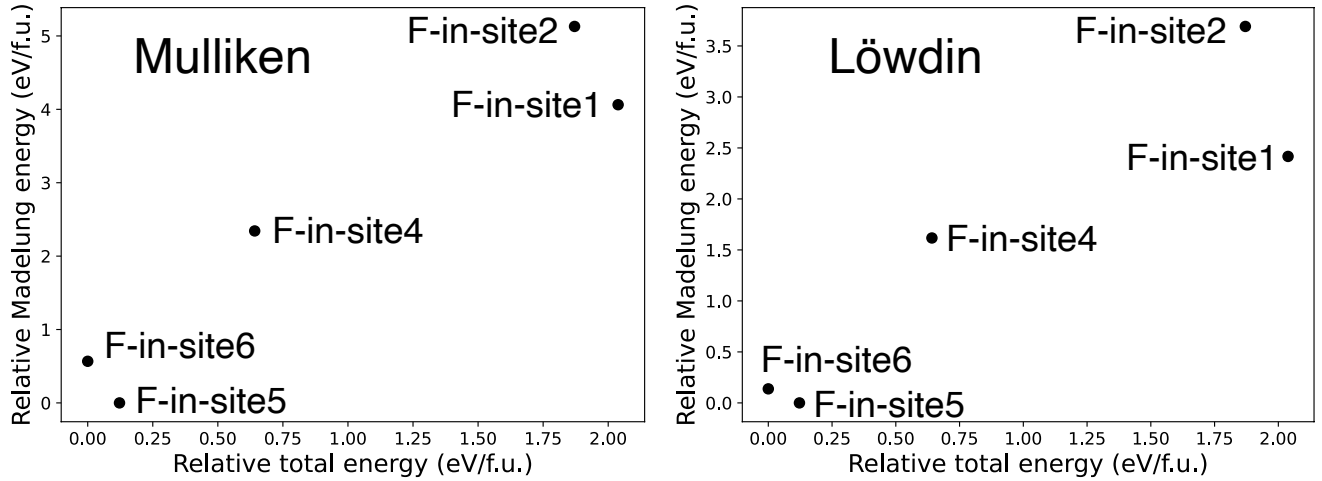


FIG. 5. The Madelung potentials calculated with Milliken and Löwdin charges. The values are plotted against the total energy. The potential and energy are given as the differences from those of the F-in-site6.

in-site5. This is a significant origin of the F-in-site6 preference in $\text{Pb}_2\text{Ti}_4\text{O}_9\text{F}_2$, which cannot be fully explained by the Pauling's second low.

V. CONCLUSION

To understand the cause of the F^- ordering, preferably occupying a specific site, $\text{Bi}_2\text{Ti}_4\text{O}_{11}$ and $\text{Pb}_2\text{Ti}_4\text{O}_9\text{F}_2$ were simultaneously investigated by SXRD technique and ab initio calculations. In $\text{Bi}_2\text{Ti}_4\text{O}_{11}$, the tetragonal instability and the accompanying anisotropic coordination result in an antiferroelectric transition. Meanwhile, $\text{Pb}_2\text{Ti}_4\text{O}_9\text{F}_2$ does not undergo an antiferroelectric transition down to 5 K, because F^- selectively occupies the closest anion site (site-6) to Bi/Pb, and then F^- elongates the Bi/Pb-O/F6 distance and reduces the distortion around the Bi/Pb. We found that the binding hybridization between Pb-6s and F6-2p is significantly weaker than Bi-6s and O6-2p, explaining the longer distance of Pb-F6 than Bi-O6. Ab initio calculations were performed to analyze the F-in-site6 preference. Though the F-in-site6 is surely observed experimentally to be the most stable configuration, it is not fully explained by the electrostatic (Madelung) potential, being an exception of Pauling's second rule. To understand the reason, we focus on the orbital energies. The PDOS analysis shows that the O2-2p is significantly more stable for F-in-site6 than F-in-site5. From the structural and COHP analyses, we conclude that the anti-bonding hybrid orbital between Pb and O/F6, explained by the RLP model [47], hampers the bind-

ing between Pb and O2 more strongly for the F-in-site5 than F-in-site6.

ACKNOWLEDGMENTS

The synchrotron radiation experiments were performed at the BL02B2 of SPring-8 with the approval of the Japan Synchrotron Radiation Research Institute (JASRI) (Proposal No. 2016A1157 and No. 2018A1227). The ab initio calculations were performed with the computational resources of the Research Center for Advanced Computing Infrastructure (RCACI) at JAIST. T.I. and F.A.R. acknowledge support from US Department of Energy, Office of Science, Basic Energy Sciences, Materials Sciences and Engineering Division. This work was also partially supported by a Grant-in-Aid for Scientific Research on Innovative Area "Mixed Anion (Project, JP17H05489, JP19H04706)" (JSPS), and a Grant-in-Aids for Scientific Research (C) (Project JP16K05731 and 21K04659). K.H. is grateful for financial support from the HPCI System Research Project (Project ID: hp190169), MEXT-KAKENHI (JP16H06439, JP17K17762, JP19K05029, and JP19H05169), and the Air Force Office of Scientific Research (Award Numbers: FA2386-20-1-4036). R.M. is grateful for financial supports from MEXT-KAKENHI (JP19H04692 and JP16KK0097), FLAGSHIP2020 (project nos. hp190169 and hp190167 at K-computer), the Air Force Office of Scientific Research (AFOSR-AOARD/FA2386-17-1-4049; FA2386-19-1-4015), and JSPS Bilateral Joint Projects (with India DST).

[1] H. Kageyama, K. Hayashi, K. Maeda, J. P. Attfield, Z. Hiroi, J. M. Rondinelli, and K. R. Poeppelmeier, Expanding frontiers in materials chemistry and physics with multiple anions, *Nat Commun* **9**, 772 (2018).

[2] R. Kuriki, T. Ichibha, K. Hongo, D. Lu, R. Maezono, H. Kageyama, O. Ishitani, K. Oka, and K. Maeda, A stable, narrow-gap oxyfluoride photocatalyst for visible-light hydrogen evolution and carbon dioxide reduction, *Journal of the*

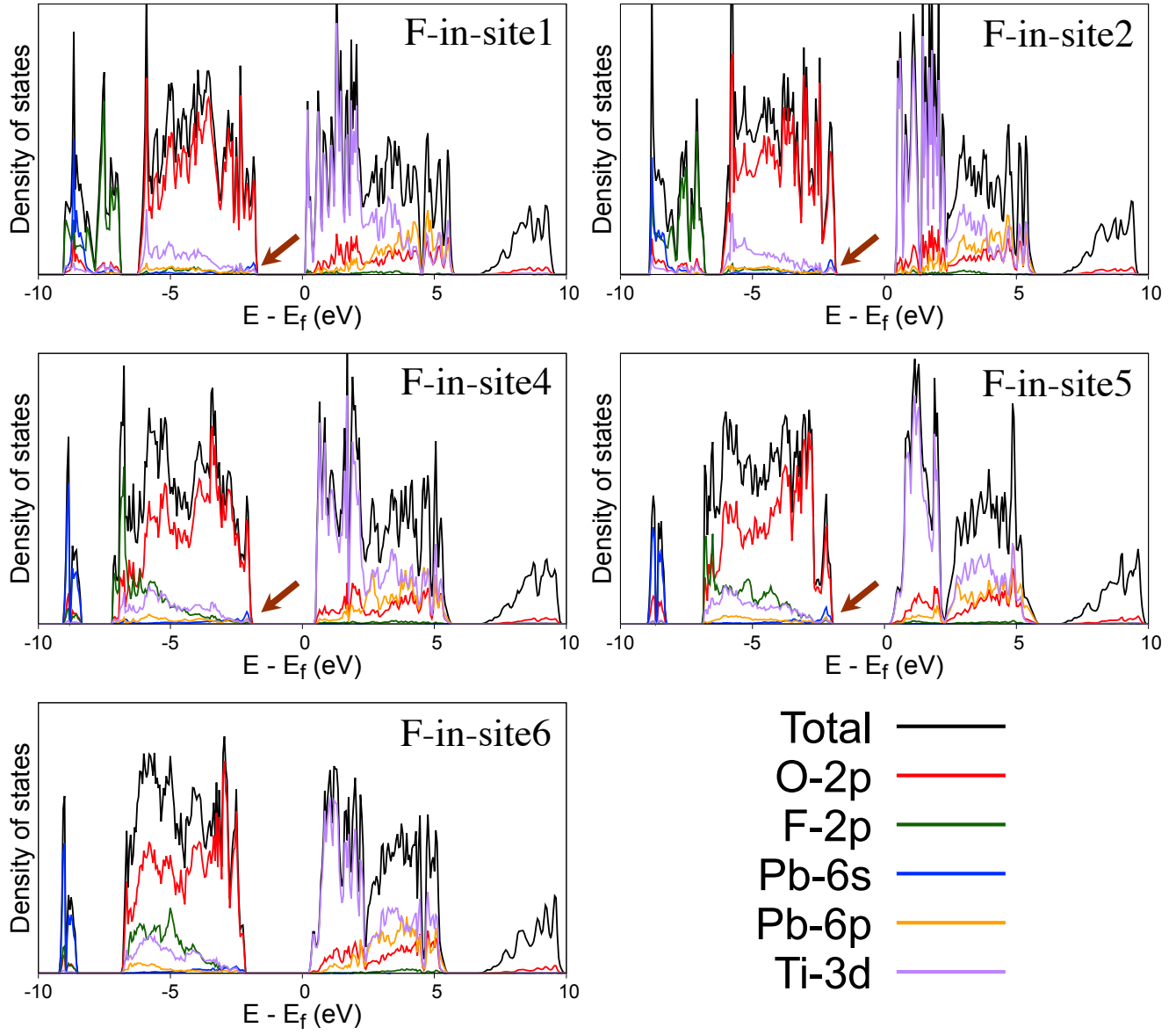


FIG. 6. Partial density of states predicted by DFT. The arrows indicate the peaks accompanied by the Pb-6s peaks.

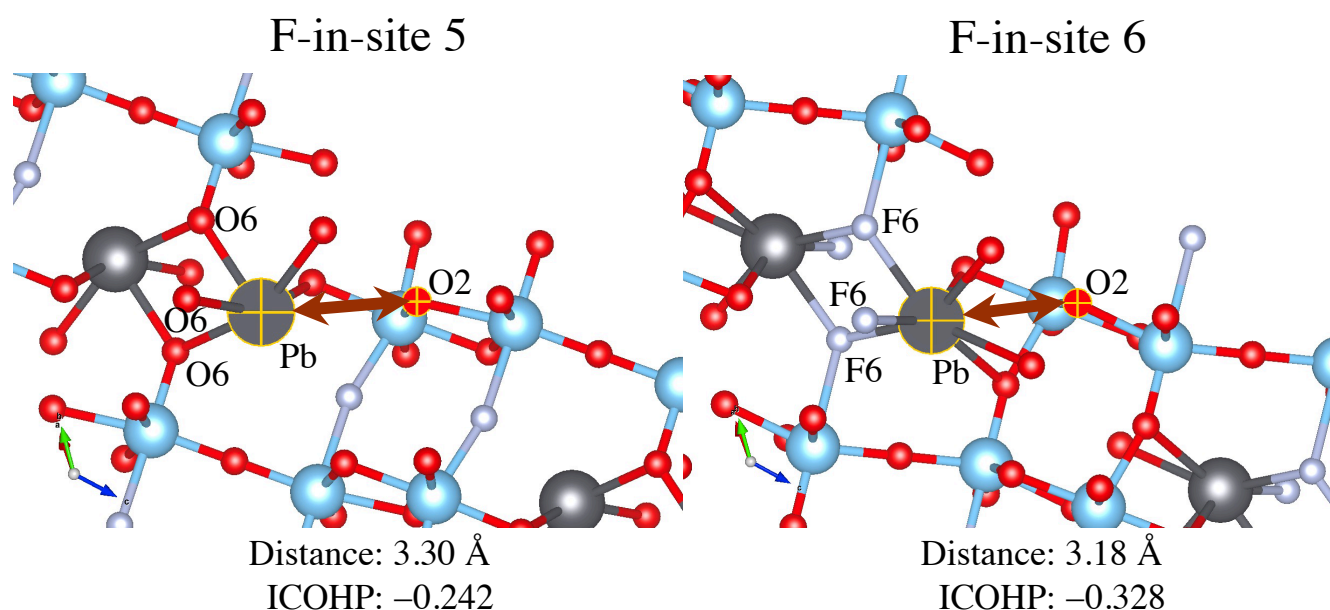


FIG. 7. The crystal structures around the Pb and O2 of the F-in-site5 and F-in-site6.

- American Chemical Society **140**, 6648 (2018).
- [3] T. Oshima, T. Ichibha, K. S. Qin, K. Muraoka, J. J. M. Vequizo, K. Hibino, R. Kuriki, S. Yamashita, K. Hongo, T. Uchiyama, K. Fujii, D. Lu, R. Maezono, A. Yamakata, H. Kato, K. Kimoto, M. Yashima, Y. Uchimoto, M. Kakihana, O. Ishitani, H. Kageyama, and K. Maeda, Undoped layered perovskite oxynitride $\text{Li}_2\text{La}_2\text{O}_6\text{N}$ for photocatalytic CO_2 reduction with visible light, *Angewandte Chemie International Edition* **57**, 8154 (2018), <https://onlinelibrary.wiley.com/doi/pdf/10.1002/anie.201803931>.
 - [4] T. Oshima, T. Ichibha, K. Oqmhula, K. Hibino, H. Mogi, S. Yamashita, K. Fujii, Y. Miseki, K. Hongo, D. Lu, R. Maezono, K. Sayama, M. Yashima, K. Kimoto, H. Kato, M. Kakihana, H. Kageyama, and K. Maeda, Two-dimensional perovskite oxynitride $\text{K}_2\text{La}_2\text{O}_6\text{N}$ with an h^+/k^+ exchangeability in aqueous solution forming a stable photocatalyst for visible-light H_2 evolution, *Angewandte Chemie International Edition* **59**, 9736 (2020), <https://onlinelibrary.wiley.com/doi/pdf/10.1002/anie.202002534>.
 - [5] Y.-I. Kim, P. M. Woodward, K. Z. Baba-Kishi, and C. W. Tai, Characterization of the structural, optical, and dielectric properties of oxynitride perovskites AMO_2N ($a = \text{Ba, Sr, Ca}$; $m = \text{Ta, Nb}$), *Chemistry of Materials* **16**, 1267 (2004).
 - [6] K. Page, M. W. Stoltzfus, Y.-I. Kim, T. Proffen, P. M. Woodward, A. K. Cheetham, and R. Seshadri, Local atomic ordering in BaTaO_2N studied by neutron pair distribution function analysis and density functional theory, *Chemistry of Materials* **19**, 4037 (2007).
 - [7] M. Yang, J. Oró-Solé, J. A. Rodgers, A. B. Jorge, A. Fuertes, and J. P. Attfield, Anion order in perovskite oxynitrides, *Nature Chemistry* **3**, 47 (2010).
 - [8] T. Yamamoto, D. Zeng, T. Kawakami, V. Arcisauskaite, K. Yata, M. A. Patino, N. Izumo, J. E. McGrady, H. Kageyama, and M. A. Hayward, The role of π -blocking hydride ligands in a pressure-induced insulator-to-metal phase transition in SrVO_2H , *Nature Communications* **8**, 10.1038/s41467-017-01301-0 (2017).
 - [9] C. M. Thompson, C. K. Blakely, R. Flacau, J. E. Greedan, and V. V. Poltavets, Structural and magnetic behavior of the cubic oxyfluoride SrFeO_2F studied by neutron diffraction, *Journal of Solid State Chemistry* **219**, 173 (2014).
 - [10] F. J. Berry, F. C. Coomer, C. Hancock, c. Helgason, E. A. Moore, P. R. Slater, A. J. Wright, and M. F. Thomas, Structure and magnetic properties of the cubic oxide fluoride BaFeO_2F , *Journal of Solid State Chemistry* **184**, 1361 (2011).
 - [11] T. Katsumata, M. Nakashima, H. Umemoto, and Y. Inaguma, Synthesis of the novel perovskite-type oxyfluoride PbScO_2F under high pressure and high temperature, *Journal of Solid State Chemistry* **181**, 2737 (2008).
 - [12] R. L. Needs and M. T. Weller, A new $2+/3+$ perovskite: The synthesis and structure of BaScO_2F , *Journal of Solid State Chemistry* **139**, 422 (1998).
 - [13] F. Takeiri, T. Yamamoto, N. Hayashi, S. Hosokawa, K. Arai, J. Kikkawa, K. Ikeda, T. Honda, T. Otomo, C. Tassel, K. Kimoto, and H. Kageyama, AgFeO_2F : A fluorine-rich perovskite oxyfluoride, *Inorg Chem* **57**, 6686 (2018).
 - [14] T. Katsumata, R. Suzuki, N. Satoh, S. Suzuki, M. Nakashima, Y. Inaguma, D. Mori, A. Aimi, and Y. Yoneda, Synthesis of new perovskite-type oxyfluorides, BaInO_2F and comparison of the structure among perovskite-type oxyfluorides, *Journal of Solid State Chemistry* **279**, 120919 (2019).
 - [15] Y. Inaguma, K. Sugimoto, and K. Ueda, Synthesis of the perovskite-type oxyfluoride AgTiO_2F : an approach adopting the hsbp principle, *Dalton Transactions* **49**, 6957 (2020).
 - [16] M. Ai-Mamouri, P. P. Edwards, C. Greaves, and M. Slaski, Synthesis and superconducting properties of the strontium copper oxy-fluoride $\text{Sr}_2\text{CuO}_2\text{F}_{2+\delta}$, *Nature* **369**, 382 (1994).
 - [17] G. Simon Case, A. L. Hector, W. Levason, R. L. Needs, M. F. Thomas, and M. T. Weller, Syntheses, powder neutron diffraction structures and Mössbauer studies of some complex

- iron oxyfluorides: Sr₃Fe₂O₆F_{0.87}, Sr₂FeO₃F and Ba₂FeO₅F_{0.68}, *Journal of Materials Chemistry* **9**, 2821 (1999).
- [18] A. L. Hector, J. A. Hutchings, R. L. Needs, M. F. Thomas, and M. T. Weller, Structural and mössbauer study of Sr₂FeO₃x (x = f, cl, br) and the magnetic structure of Sr₂FeO₃F, *Journal of Materials Chemistry* **11**, 527 (2001).
- [19] R. L. Needs and M. T. Weller, Synthesis and structure of Ba₂InO₃F: oxide/fluoride ordering in a new K₂NiF₄ superstructure, *Journal of the Chemical Society, Chemical Communications*, 353 (1995).
- [20] R. L. Needs, M. T. Weller, U. Scheler, and R. K. Harris, Synthesis and structure of Ba₂InO₃x (x = f, cl, br) and Ba₂ScO₃F: oxide/halide ordering in K₂NiF₄-type structures, *Journal of Materials Chemistry* **6**, 1219 (1996).
- [21] Y. Su, Y. Tsujimoto, Y. Matsushita, Y. Yuan, J. He, and K. Yamaura, High-pressure synthesis, crystal structure, and magnetic properties of Sr₂MnO₃F: A new member of layered perovskite oxyfluorides, *Inorganic Chemistry* **55**, 2627 (2016).
- [22] Y. Tsujimoto, K. Yamaura, N. Hayashi, K. Kodama, N. Igawa, Y. Matsushita, Y. Katsuya, Y. Shirako, M. Akaogi, and E. Takayama-Muromachi, Topotactic synthesis and crystal structure of a highly fluorinated ruddlesden–popper-type iron oxide, Sr₃Fe₂O₅+x/2–x (x ~ 0.44), *Chemistry of Materials* **23**, 3652 (2011).
- [23] L.-S. Du, F. Wang, and C. P. Grey, High-resolution ¹⁹F mas and ¹⁹F–¹¹³Cd redox nmr study of oxygen/fluorine ordering in oxyfluorides, *Journal of Solid State Chemistry* **140**, 285 (1998).
- [24] Y. Inaguma, J.-M. Greneche, M.-P. Crosnier-Lopez, T. Katsumata, Y. Calage, and J.-L. Fourquet, Structure and mössbauer studies of f-o ordering in antiferromagnetic perovskite PbFeO₂F, *Chemistry of Materials* **17**, 1386 (2005), <https://doi.org/10.1021/cm048125g>.
- [25] T. Katsumata, M. Nakashima, Y. Inaguma, and T. Tsurui, Synthesis of new perovskite-type oxyfluoride, PbMnO₂F, *Bulletin of the Chemical Society of Japan* **85**, 397 (2012).
- [26] R. E. Cohen, Origin of ferroelectricity in perovskite oxides, *Nature* **358**, 136 (1992).
- [27] P. Baettig, C. F. Schelle, R. LeSar, U. V. Waghmare, and N. A. Spaldin, Theoretical prediction of new high-performance lead-free piezoelectrics, *Chemistry of Materials* **17**, 1376 (2005).
- [28] P. Ravindran, R. Vidy, A. Kjekshus, H. Fjellvåg, and O. Eriksson, Theoretical investigation of magnetoelectric behavior in BiFeO₃, *Phys. Rev. B* **74**, 224412 (2006).
- [29] Y. Inaguma, K. Ueda, T. Katsumata, and Y. Noda, Low-temperature formation of Pb₂O₂F₂ with o/f anion ordering by solid state reaction, *Journal of Solid State Chemistry* **277**, 363 (2019).
- [30] K. Oka and K. Oh-ishi, Observation of anion order in Pb₂Ti₄O₉F₂, *Inorganic Chemistry* **54**, 10239 (2015).
- [31] K. Oka, H. Hojo, M. Azuma, and K. Oh-ishi, Temperature-independent, large dielectric constant induced by vacancy and partial anion order in the oxyfluoride pyrochlore Pb₂Ti₂O_{6–δ}F_{2δ}, *Chemistry of Materials* **28**, 5554 (2016).
- [32] A. L. Hector and S. B. Wiggin, Synthesis and structural study of stoichiometric Bi₂Ti₂O₇ pyrochlore, *Journal of Solid State Chemistry* **177**, 139 (2004).
- [33] S. Hull, S. T. Norberg, M. G. Tucker, S. G. Eriksson, C. E. Mohn, and S. Stølen, Neutron total scattering study of the δ and β phases of Bi₂O₃, *Dalton Transactions*, 8737 (2009).
- [34] V. Kahlenberg and H. Böhm, The structures of [α]- and [β]-Bi₂Ti₄O₁₁, *Acta Crystallographica Section B* **51**, 11 (1995).
- [35] S. Kawaguchi, M. Takemoto, K. Osaka, E. Nishibori, C. Moriyoshi, Y. Kubota, Y. Kuroiwa, and K. Sugimoto, High-throughput powder diffraction measurement system consisting of multiple mythen detectors at beamline bl02b2 of spring-8, *Review of Scientific Instruments* **88**, 085111 (2017), <https://doi.org/10.1063/1.4999454>.
- [36] F. Izumi and K. Momma, Three-dimensional visualization in powder diffraction, *Solid State Phenomena* **130**, 15 (2007).
- [37] K. Momma, T. Ikeda, A. A. Belik, and F. Izumi, Dysnomia, a computer program for maximum-entropy method (mem) analysis and its performance in the mem-based pattern fitting, *Powder Diffraction* **28**, 184 (2013).
- [38] K. Momma and F. Izumi, Vesta 3 for three-dimensional visualization of crystal, volumetric and morphology data, *Journal of Applied Crystallography* **44**, 1272 (2011).
- [39] P. Giannozzi, S. Baroni, N. Bonini, M. Calandra, R. Car, C. Cavazzoni, D. Ceresoli, G. L. Chiarotti, M. Cococcioni, I. Dabo, A. D. Corso, S. de Gironcoli, S. Fabris, G. Fratesi, R. Gebauer, U. Gerstmann, C. Gougoussis, A. Kokalj, M. Lazzeri, L. Martin-Samos, N. Marzari, F. Mauri, R. Mazzarello, S. Paolini, A. Pasquarello, L. Paulatto, C. Sbraccia, S. Scandolo, G. Sclauzero, A. P. Seitsonen, A. Smogunov, P. Umari, and R. M. Wentzcovitch, QUANTUM ESPRESSO: a modular and open-source software project for quantum simulations of materials, *Journal of Physics: Condensed Matter* **21**, 395502 (2009).
- [40] J. P. Perdew, K. Burke, and M. Ernzerhof, Generalized Gradient Approximation Made Simple, *Phys. Rev. Lett.* **77**, 3865 (1996).
- [41] G. Kresse and D. Joubert, From ultrasoft pseudopotentials to the projector augmented-wave method, *Phys. Rev. B* **59**, 1758 (1999).
- [42] R. Nelson, C. Ertural, J. George, V. L. Deringer, G. Hautier, and R. Dronskowski, Lobster: Local orbital projections, atomic charges, and chemical-bonding analysis from projector-augmented-wave-based density-functional theory, *Journal of Computational Chemistry* **41**, 1931 (2020), <https://onlinelibrary.wiley.com/doi/pdf/10.1002/jcc.26353>.
- [43] S. Maintz, V. L. Deringer, A. L. Tchougréeff, and R. Dronskowski, Analytic projection from plane-wave and PAW wavefunctions and application to chemical-bonding analysis in solids, *Journal of Computational Chemistry* **34**, 2557 (2013).
- [44] S. Maintz, V. L. Deringer, A. L. Tchougréeff, and R. Dronskowski, LOBSTER: A tool to extract chemical bonding from plane-wave based DFT, *Journal of Computational Chemistry* **37**, 1030 (2016).
- [45] L. Nistor, G. Van Tendeloo, S. Amelinckx, V. Kahlenberg, and H. Böhm, In situ study of the phase transition in Bi₂Ti₄O₁₁, *Journal of Solid State Chemistry* **119**, 281 (1995).
- [46] Y. Kurauchi, T. Katayama, A. Chikamatsu, and T. Hasegawa, Two-dimensional fluorine distribution in a heavily distorted perovskite nickel oxyfluoride revealed by first-principles calculation, *The Journal of Physical Chemistry C* **123**, 31190 (2019), <https://doi.org/10.1021/acs.jpcc.9b09112>.
- [47] A. Walsh, D. J. Payne, R. G. Egdell, and G. W. Watson, Stereochemistry of post-transition metal oxides: revision of the classical lone pair model, *Chem. Soc. Rev.* **40**, 4455 (2011).